Monomers from CO2

Superbases as Catalysts for Formate-to-Oxalate Coupling

Schuler, E.; Ermolich, P.A.; Shiju, N.R.; Gruter, G.-J.M.

DOI
10.1002/cssc.202002725

Publication date
2021

Document Version
Final published version

Published in
ChemSusChem

Monomers from CO_2: Superbases as Catalysts for Formate-to-Oxalate Coupling

Eric Schuler,*[a] Pavel A. Ermolich,[a] N. Raveendran Shiju,[a] and Gert-Jan M. Gruter*[a, b]

An interesting contribution to solving the climate crisis involves the use of CO_2 as a feedstock for monomers to produce sustainable plastics. In the European Horizon 2020 project "OCEAN" a continuous multistep process from CO_2 to oxalic acid and derivatives is developed, starting with the electrochemical reduction of CO_2 to potassium formate. The subsequent formate-to-oxalate coupling is a reaction that has been studied and commercially used for over 150 years. With the introduction of superbases as catalysts under moisture-free conditions unprecedented improvements were shown for the formate coupling reaction. With isotopic labelling experiments the presence of carbonite as an intermediate was proven during the reaction, and with a unique operando set-up the kinetics were studied. Ultimately, the required reaction temperature could be dropped from 400 to below 200 °C, and the reaction time could be reduced from 10 to 1 min whilst achieving 99% oxalate yield.

Introduction

Formate coupling to oxalate is an old reaction first discovered in 1852 and was the main commercial way to produce oxalic acid before the advent of petrochemical routes.[1–3] With the ambition of the society to decrease atmospheric CO_2 levels, the Carbon Capture and Utilization (CCU) approach to produce chemicals from CO_2 is receiving significant interest.[4–10] Although considerable progress has been made towards converting CO_2 to formate through direct hydrogenation or hydrothermal-chemical reduction in water, in the "OCEAN" project we focus on the electrochemical reduction of CO_2 to formate and CO, which does not require hydrogen and elevated temperature.[11,12] As formate and CO can both be obtained via a 2-electron electrochemical reduction of CO_2, the electrochemical production of formate from CO_2 aligns well with the ambition to use CO_2 as a renewable C_1 feedstock.[13,14] In addition, CO_2 can have a low or even negative cost and high abundance.[15–17] In the "OCEAN" project we use the CO_2-to-formate reaction and the formate product tree as a stepping stone towards large scale electrochemical conversion of CO_2 and H_2O to syngas, the starting point for many downstream products, including chemicals, polymers, and fuels.[7,18,19] Polymers can be especially interesting as they allow for long-term storage of sequestered CO_2 in materials.[15,16] CO_2-based chemicals such as oxalic acid will become new platform chemicals for a wide range of downstream products such as mono-ethylene glycol (MEG) as well as glycolic and glyoxylic acid that all can be obtained from oxalic acid.[20]

Once formate is made from CO_2, a high-performing process for the coupling of formate to oxalate will bridge the gap between CO_2 reduction and the large-scale utilization of this CO_2-derived carbon in new chemical products with negative CO_2 footprints. This work is part of the European Horizon 2020 project "OCEAN" in which we develop a continuous process from CO_2 to polymers.[21] The first step in the "OCEAN" process involves the electrochemical reduction of CO_2 to potassium formate. Potassium was selected as the counter ion because it gives by far the best reduction efficiency.[22,23] The potassium formate can be effectively recovered from the solution by a combination of evaporation and cooling crystallization. We then take this potassium formate and subject it to a coupling reaction to form oxalate. We report here our results of this second step from the CO_2 conversion chain to polymers as shown in Figure 1.

Commercially, the formate coupling reaction (FCR) is performed at high temperatures of 380–420 °C using hydroxides as catalysts.[24–27] With these hydroxide bases, the reaction takes

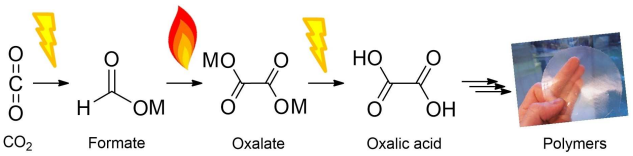

Figure 1. "OCEAN" process for CO_2 utilization via electrochemical reduction to formate, thermal formate coupling to oxalate, electrochemical oxalate acidification, and polymer production from oxalic acid and its derivates.

[a] E. Schuler, P. A. Ermolich, Dr. N. R. Shiju, Prof. G.-J. M. Gruter
Van 't Hoff Institute for Molecular Sciences
University of Amsterdam
Science Park 904, 1090 GD Amsterdam
(The Netherlands)
E-mail: e.schuler@uva.nl
g.j.m.gruter@uva.nl
[b] Prof. G.-J. M. Gruter
Avantium Chemicals BV
Zekeringstraat 29, 1014 BV Amsterdam
(The Netherlands)

Supporting information for this article is available on the WWW under https://doi.org/10.1002/cssc.202002725

more than 30 min to proceed, but reaction temperatures are high and oxalate yields are not optimal. Especially the production of carbonate as a side product is problematic as it requires the introduction of a downstream separation step. The reaction kinetics as a function of process conditions was extensively studied in the 1930s in Russia by Freidlin et al.[28–40] In the 1970–80s Shishido and Masuda[41,42] as well as Górski and Kraśnicka[43–46] investigated the coupling reaction focusing on the decomposition products and the reaction mechanism. Recently, the FCR as part of CCU pathways gained new interest, and several new patents and studies were published in China.[47–58] A recent publication on the topic was from Lakkaraju et al. who introduced hydrides as catalyst and presented a new mechanism.[59] Our work was initially sparked by the many questions still open after reading the previous publications. We explored alternative catalysts, mainly the superbases (SB) such as lithium, sodium, and potassium hydride as well as sodium amide (NaH, KH, LiH, and $NaNH_2$), optimized the reaction conditions, studied kinetics and mechanisms, and found an optimal alternative process for the FCR.

Results and Discussion

In the quest of finding new catalysts that can decrease the reaction temperature and time, we first tried to understand the FCR reaction better by looking at the probable mechanism. Many reaction mechanisms have been proposed, and most recently Lakkaraju et al. suggested carbonite (COO^{2-}) as the key intermediate species as shown in Scheme 1.[59]

This is an interesting study from the mechanistic point of view; however, no significant improvements in terms of selectivity, reaction time, and reaction temperature were reported. We first tried to follow the reaction with Raman spectroscopy (see Figure 2A). However, we were not able to see the carbonite peak at any given configuration. We then used isotope labelling studies. With excess catalyst, the carbonite lifetime increases due to a reduced formate (reaction partner) concentration, as shown with Raman studies by Lakkaraju et al.[59] We first produced carbonite by adding an excess amount of hydride. The carbonite prevails as it does not find a reaction partner. We then introduced D_2O as a reaction partner, which reacted with carbonite to form deuterated formate

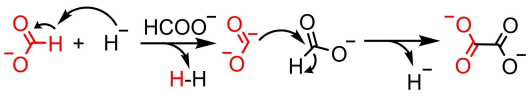

Scheme 1. FCR promoted by base catalysts with carbonite as intermediate as suggested by Lakkaraju et al.[59]

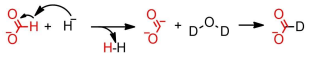

Scheme 2. Reaction pathway for isotope labelling of carbonite intermediate with D_2O.

($DCOO^-$; see Scheme 2). The reaction was quenched after completion. The only species observed in a GC–MS (with electrospray ionization) of the quenched sample had a *m/z* of 46 corresponding to deuterated formate ($DCOO^-$). We also did two control reactions: (1) quenching the reaction with water, and (2) adding D_2O to formate without performing the coupling reaction. In both cases, we observed *m/z* of 45 corresponding to formate ($HCOO^-$).

The formation of the carbonite being the rate-limiting step explains the need for a strong base to extract the proton from the formate ($HCOO^-$) anion. Their catalytic activity relies on their intrinsic property of strong basicity and not on complex molecular or surface structures such as in homogeneous or heterogeneous catalysts, respectively. Based on this insight, we tested compounds well known for their basic properties and compared them to hydroxides, the state-of-the-art catalyst since 1882.[60,61] We did these tests under inert conditions using home-build high-speed kinetic measurement equipment based on the work of Slot et al. connected with operando Raman spectroscopy and gas analysis capabilities.[62]

Our results shown in Table 1 indicate that four catalysts, LiH, NaH, KH, and $NaNH_2$, show excellent activity due to their superbase properties. These catalysts are superior in oxalate yield and allow the reaction to proceed 10 times faster at temperatures 200 °C lower than that used with hydroxides. The catalysts gave yields of up to 97 %, with reaction occurring soon after melting of the substrate (169 °C) and going to completion in 1–3 min.

For all catalysts, the reactions were performed at varying temperatures and the achieved oxalate yields, as measured by both LC and IR spectroscopy, are shown in Figure 2B. Without catalyst, the reaction starts at 360 °C, reaching yields of up to 21 % at 420 °C; however, the required reaction time as shown in Figure 2D exceeds 3 h.

Hydroxide catalyst speeds up the reaction to 30 min and lowers the required reaction temperature to 410–430 °C. Early patents for batch processes report even longer times of up to 6 h.[63–66] When reacting potassium formate with hydroxide bases, only 63 % oxalate yield could be achieved. The reduced

Table 1. Performance indicators of catalysts for coupling of potassium formate.

Catalyst	Reaction onset *T* [°C]	Ideal reaction *T*[a] [°C]	Oxalate yield[b] [%]	Reaction time[c] [min]
NaH[d]	350	380–420	99	10
NaH	153	180–200	95	0.5–2
KH	153	180–200	97	1–2
LiH	153	180–200	95	1-2
$NaNH_2$	154	180–200	95	<1
$NaBH_4$	320	335–360	88	5–15
KOH	327	410–430	63	10–30
–	360	420–440	21	150–200

[a] Temperature at which highest yields were achieved. [b] Highest yield achieved with 2.5 wt% catalyst loading. [c] Time at which 90 % conversion was achieved. [d] Reference from Lakkaraju et al. using sodium formate and NaH as catalyst.[59] The reaction was observed at 350 °C. No observation of reaction start at melting point of formate.

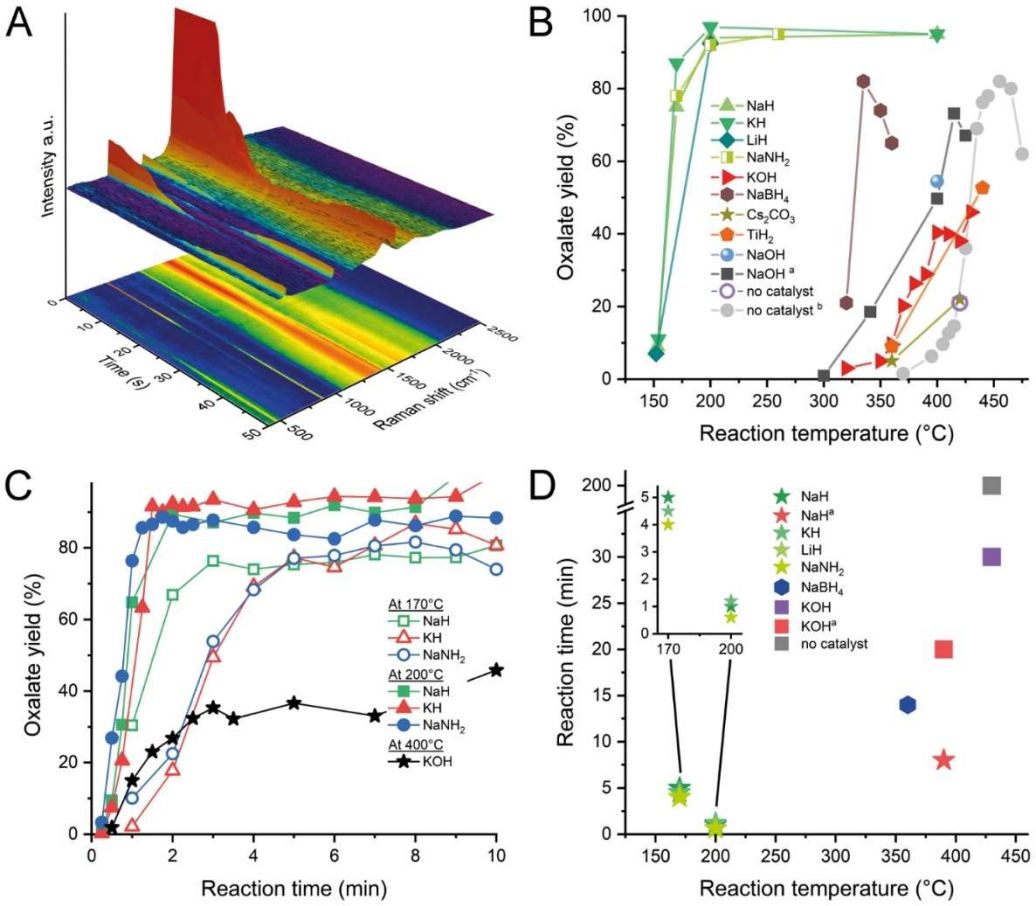

Figure 2. A) Time-resolved Raman spectrum from formate coupling reaction using 10 wt% NaH at 200 °C in a pre-heated reactor. The first 10 s are not shown as they represent the heat-up time of the reactor. The peaks at 770, 1084, 1342, 1364, and 1532 cm^{-1} can be attributed to formate. These disappear within 25 s, after which peaks of oxalate appear at 467, 881, 1437, and 1617 cm^{-1}. The peak indicative of carbonite at 1076 cm^{-1} did not appear during or after the reaction. B) Oxalate yields at different reaction temperatures for the potassium formate coupling reaction are plotted for all tested catalysts accompanied by two literature values. Each datapoint represents a single experiment at the given temperature in a pre-heated reactor and not temperature profiles. At the end, the oxalate yield was determined by IR spectroscopy and LC measurements. SB-catalyzed reactions showed great improvements in yield at low temperatures. [a] Sodium formate with sodium hydroxide values from Freidlin.[35] [b] Non-catalyzed potassium values from Freidlin.[31] C) Oxalate yields obtained with instantaneous heating in pre-heated reactor, each datapoint represents an individual reaction quenched after the given time. Higher oxalate yields in FCR with SBs are obtained faster at 200 °C compared to reactions at 170 °C (melting of reactant). However, hydroxide-catalyzed FCR is much slower even at 400 °C. D) Dependency of reaction times on the reaction temperature. All reaction times correspond to the point when >90% conversion was reached. Higher temperatures and stronger bases reduce the reaction times drastically by up to 200 times compared to non-catalyzed reactions and 30 times compared to the conventional KOH catalyst. [a] Values reported by Lakkaraju et al.[59]

yield can partly be explained by side reaction [Eq. (1)] and product decomposition reaction [Eq. (2)] towards carbonate.

$$HCOOK + KOH \rightarrow K_2CO_3 + H_2 \quad (1)$$

$$K_2C_2O_4 + 2\ KOH \rightarrow 2\ K_2CO_3 + H_2 \quad (2)$$

The yields with our superbase catalysts are very high at 99% but not higher than the literature values reported with sodium formate as reactant; however, the rate of the reaction is higher, and the reaction temperature is much lower.[35,59] Moreover, no formation of carbonate as a side-product was observed with our superbase catalysts, and the reaction follows a zero-order regime throughout. The confirmed presence of carbonite when SBs were used supports the Lakkaraju mechanism, but our observation that the reactions proceed at 200 °C lower temperatures emphasizes the importance of an absolutely moisture- and oxygen-free reaction environment. In the presence of (small amounts) of water, the hydrides (present at low concentrations) are converted to hydroxides, requiring conventional reaction temperatures (300–400 °C). We also noticed dependency of oxalate yields on counter-ions as well as reactor designs. We currently investigate this dependency and will report mechanistic reasons as well as solutions in upcoming publications.

When using a temperature profile starting at 25 °C and heating at 1 °C min^{-1}, the reaction starts from a low temperature (≈153 °C) for the superbases and reaches maximum rate around the melting of formate (169 °C). The fast reaction upon melting and similar behaviour of all SBs, despite their difference in basicity, suggest the possibility of even lower reaction temperatures, if the melting temperature could be lowered. This would be one of the future directions to study.

Strong foaming through the hydrogen evolution during the vigorous start of the reaction causes solidification of the product as a foamed-up structure (shown in Figure S4). This fast reaction does not give enough time for efficient mass transfer and mixing and thereby encapsulates some unreacted formate. Therefore, adequate mixing of the reactant and catalyst for example by milling is important as the reaction proceeds quickly upon melting. In our set-up, temperatures of 200 °C were required to achieve the maximum yield.

Below this temperature the conversion was not complete and proceeded slower as shown in Figure 2C. Moreover, the heating rate is also of great importance as it can significantly influence the oxalate yield.[45] Slower heating rates of 0.25–2 °C min^{-1} ensure better gas escape through the reactant particles and prevent the puffing, leading to a tightly packed product at the bottom of a reaction vial with a high yield at 170 °C (Figure S4). However, this comes with the consequence of longer residence times for reaction completion.

Although inert conditions in the absence of oxygen are important to prevent oxidative side reactions to carbonates for FCR in general, the absolute absence of water is crucial for SBs. The presence of water leads to decomposition reactions as in Scheme 3, losing the advantage of superbase.

The minimum catalyst required for the reaction is hence heavily influenced by the dryness of the reactor and reactants. At our small scale (290–310 mg of substrate per experiment) we needed a minimum catalyst loading between 0.05 and 0.2 wt%, which can be attributed to varying amounts of moisture still remaining in the substrate. With loadings above 1 wt%, the reaction proceeded at its maximum speed for all SBs. Unlike hydroxides, there are no side reactions when using SBs, and consequently no carbonate or any other side-product was observed for temperatures up to 450 °C. Above 450 °C oxalate decomposes to carbonate and CO. However, these temperatures are never required for the reactions with SBs.

Metal hydrides such as TiH_2, MgH_2, and $NaBH_4$ are commonly used for hydrogen storage. We tested them as catalysts for the FCR but did not observe catalytic activity for TiH_2 and MgH_2 and slightly higher activity for $NaBH_4$ compared with KOH. Metal hydrides with two hydrogen atoms attached are more stable (less basic) and more importantly do not release hydride ions, which are crucial for the reaction. Consequently, they do not catalyze the reaction. The fast liberation of hydrogen seen in Figure S6 does not reflect formate conversion as it originates form the metal hydrides. Borohydrides are also widely used in organic chemistry as a reducing agent. Their thermal stability and high basicity make them a promising candidate for the reaction. We indeed see catalytic activity starting at 285 °C with the highest yields reached at 335 °C. Above this temperature the reaction proceeds faster but the yield drops with increasing temperature. We attribute this to the decomposition of the borohydride which also causes destruction of the formed oxalate by reactive borohydride or boron species. During the decomposition of $NaBH_4$ a lot of hydrogen is also released, which explains the surplus production as shown in Figure 3C compared to the expected value obtained from FCR alone.

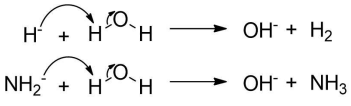

Scheme 3. Hydride and amide ion reaction with water leading to catalyst transformation to hydroxide (and deactivation).

The suitability of caesium carbonate as a base capable of proton abstraction was proposed by Banerjee and Kanan.[67] Using it in our FCR experiments, however, showed no activity beyond the self-catalyzed reaction as shown in Figure S6. Caesium carbonate is a weaker base compared to hydroxides, and thus its proton abstraction qualities are expected to be worse.

Our kinetic experiments are based on high-resolution bubble counting (example reactions shown in Figure 3A,B, set-up shown in Figure S3) connected with operando Raman measurements. For calculations of rate, reaction order, and activation energies we used the hydrogen volumetric data due to its high resolution (2000 bubbles min^{-1}) with a total number of 5000 gas bubbles for each experiment. With non-isothermal kinetic experiments in the range of 25–450 °C, Figure 3C shows the respective reaction rates, and Figure 3D shows the turnover frequencies (TOF) as calculated using Equation (S11) (low-performing catalysts are shown in Figure S6). The reaction rates for SBs exceed non-catalyzed and hydroxide-catalyzed reactions by a factor of 5 and borohydride-catalyzed reactions by a factor of 2. Sodium amide shows the highest TOF followed by sodium and potassium hydrides. Lithium hydride had a low TOF, which was caused by the fast reaction combined with a relatively higher catalyst loading. Caesium carbonate and MgO only show minor improvements on the reaction rate relative to the uncatalyzed reaction. For TiH_2 the hydrogen release coincides with the reaction start and causes a falsely high measured reaction rate.

We used Arrhenius plots to calculate the activation energy and pre-exponential factor *A* as shown in Table 2 (also more data shown in Table S1). *A* is often referred to as "frequency" factor and indicates the rate at which molecular collisions occur and therefore indicative of the contribution of a physical effect on the reaction or if the calculated activation energies are purely chemical activation values. If *A* is larger than 10^{30} s^{-1} physical diffusion limitation of the reaction is likely.[68]

The calculated activation energy for the FCR without catalyst is 196 kJ mol^{-1} and in agreement with literature

Table 2. Performance indicators of catalysts for formate coupling reaction.

Catalyst	Activation energy [kJ mol^{-1}]	*A* [s^{-1}]	Error [kJ mol^{-1}]
NaH	527	3.02×10^{67}	±5.68
KH	535	4.18×10^{67}	±5.54
LiH	814	6.54×10^{86}	±11.1
$NaNH_2$	305	3.90×10^{56}	±25.5
$NaBH_4$	266	1.09×10^{23}	–
KOH	125	1.06×10^{13}	–
HCOOK	196	1.28×10^{19}	–

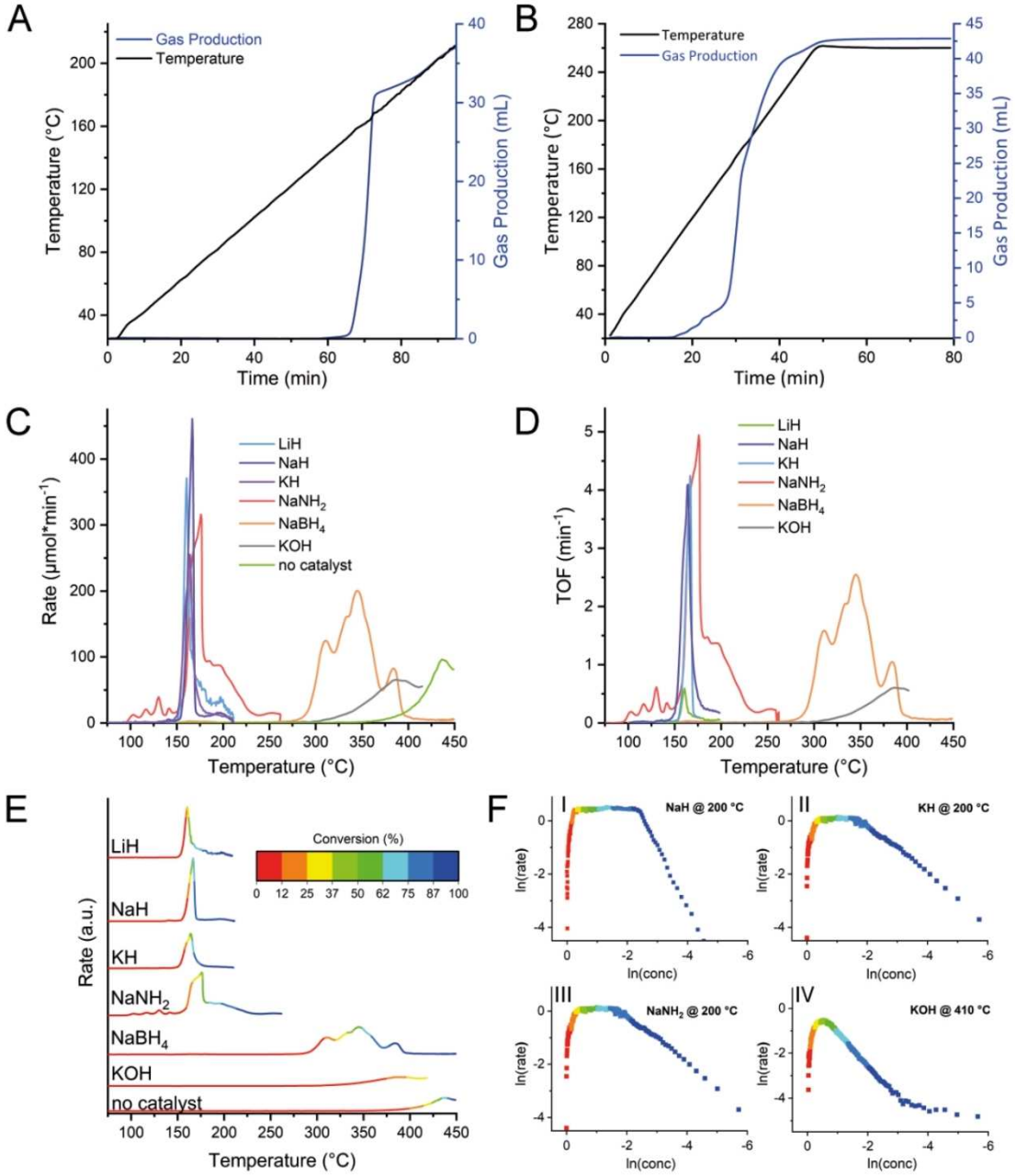

Figure 3. A) Kinetic graph obtained in a bubble counter experiment for 1 wt% NaH-catalyzed reaction with potassium formate. During the reaction the temperature is increased at a constant rate of 2 °C min^{-1}. As a measure of reaction progress the gas production from the reaction is measured using a bubble counter. The gas volume expected for full conversion of all formate to oxalate is approximately 40 mL. B) Kinetic experiment similar to A) when using 2.5 wt% $NaNH_2$ as catalyst instead. C) Reaction rates for reactions at various catalyst loadings with respect to temperature, which is increased at a constant rate of 2 °C min^{-1}. The drop of the reaction rate at increasing temperature especially for SBs originates from the completion of reaction. We are unable to provide rate data for higher temperatures as the reaction rate exceeds the physically possible heating rate of the mixture. Sodium borohydride marks an exception and has other, yet unknown, side reactions happening. D) TOFs for all successful catalysts were calculated based on the reaction rate and the catalyst loading with respect to temperature, which is increased at a constant rate of 2 °C min^{-1}. E) Reaction rates for different catalysts at different conversion stages. It becomes apparent that the reaction rate drops as expected when the reaction reaches full conversion. This is only not the case for $NaBH_4$, KOH, and the non-catalyzed reaction, which cause gas production due to decomposition. F) Logarithm of gas production during isothermal reaction plotted against the change in formate concentration to evaluate the reaction order. For reactions I, II, and III a horizontal part of the graphs corresponds to 0 reaction order (from yellow to light blue). The slope in IV is 1 as observed also for the other reactions towards full conversion (blue to dark blue).

values.[69] The low pre-exponential factor of 1.28×10^{19} s^{-1} points to absence of physical effects. Lower activation energies are expected when catalysts are used. For KOH we calculated an activation energy of 125 kJ mol^{-1}, and *A* equals 1.06×10^{13} s^{-1}. So far, only Lakkaraju et al. estimated the activation energy for a catalyzed FCR using sodium formate as reactant.[59] They used the Eyring–Polanyi equation, which gave an activation energy of approximately 177 kJ mol^{-1} and a pre-exponential factor *A* of

1.3×10^{37} s^{-1}. This indicates that their activation energy entails physical effects, which explains also the relatively high number, especially as they claim to have used hydrides. However, they required a temperature range between 330 and 420 °C; a typical range for hydroxide-catalyzed reaction, which is far above the melting point of 253 °C for the sodium formate. The increased activation energy and reaction temperature suggests that hydride was not the active species in their reactions.

In our experiments, hydrides and amides performed better at lower temperatures than hydroxides, and thus even lower activation energies were expected. However, the calculated energies are up to 5 times higher than for the hydroxide-catalyzed reaction (between 330–546 $\pm$5.6 kJ mol^{-1}; Table 2 and Table S1; plots in Figure S5). The values are independent from catalyst loading and are high, from 3.90×10^{56} to 6.54×10^{86} s^{-1}. Together with the observed coincidence of reaction onset and melting, this indicates the dominance of physical processes. These include the endothermic melting of formate, strong diffusion upon melting, mass transfer limitations from the immediate formation of solid product, and heat loss with the produced gas. Non-isothermal kinetic experiments in the same set-up revealed that SB reactions follow zero-order kinetics, which is in contrast to first order behavior observed for hydroxide-catalyzed reactions.

Figure 3F illustrates that this zero-order reaction is observed throughout 75% of the reaction and then slows down to first-order behavior, except for NaH-catalyzed reactions, which change towards second-order behavior. The zero-order reaction indicates that a truly catalytic reaction is present, and the maximum reaction rate is reached due to the strong excess of reactant over the catalyst. With the reaction progress, limited mass transfer due to the formation of solid oxalate occurs.

The first-order behavior of hydroxide-catalyzed reactions indicates a dependency on reactant concentration. The hydroxide reaction requires the in-situ generation of reactive hydride and therefore has a more complex mechanism, which we are studying now. True activation energies of the SB-catalyzed reactions require a separation of the physical effects from reaction start. This can be achieved when melting occurs before the start of reaction or when operating in a solvated system. Stirring improves mass transfer and optimal reactant mixing whilst no energy liberated by melting obstructs the measurement. To achieve this, we tried to create eutectic salt mixtures with lower melting points; we determined their melting points with differential scanning calorimetry. However, we did not observe any significant drop in the melting temperature (see also Figure S7).

Conclusion

In conclusion, we report significant improvements in reaction rates of formate coupling at low temperature using superbase (SB) catalysts. We also obtained mechanistic and kinetic insights for the reaction with isotope labelling and operando kinetic studies. We identified that reactant mixing, absence of H_2O and O_2, inert atmosphere, and slow heating are important for getting high yields with a rapid rate at low catalyst loadings. This is the first time that a significant reduction in the reaction temperature of formate coupling reaction (FCR) (from 380–420 to 170–200 °C) is reported. Additionally, the reaction times are reduced from 5–10 to 0.5–2 min whilst achieving oxalate yields of 99%. Catalyst loadings as little as 0.01 wt% proved effective, and in contrast to hydroxide-catalyzed coupling, no carbonate was formed as side product. Among several SB catalysts tested, alkali metal hydrides, amides, and borohydrides proved suitable whilst alkaline and transition-metal hydrides did not work. We detected high reaction rates for reactions catalyzed with SBs compared to traditional hydroxide catalysts. SB-catalyzed FCRs were shown to follow zero-order behavior in contrast to hydroxide- and non-catalyzed FCRs. Activation energies for non-catalyzed and hydroxide-catalyzed FCRs were measured and found to be in agreement with literature. However, we could not estimate the true chemical activation energies for SB-catalyzed reactions. The kinetics of new SB-catalyzed reactions are mainly determined by physical processes such as substrate melting and mixing of reactants; the true chemical activation energies could not be determined, as illustrated by the very high pre-exponential factors obtained. However, the results are very reproducible, also for the physical effects, and are independent of the catalyst concentration. Open questions will be addressed in an upcoming publication using experimental and computational techniques (molecular dynamics).

With respect to commercial application of our SB-based system, the lower reaction temperature, shorter residence time, and elimination of downstream separation are beneficial. Yet, the handling of superbases is more critical compared to hydroxides as the requirement of oxygen- and moisture-free conditions adds an energy-intensive formate pre-drying. Similar to the case of hydroxide catalyst, the hydride catalyst recovery is not essential. At 1% catalyst loading, the hydride catalyst cost is only a marginal part of the overall oxalic acid production cost. At larger scales we also expect a further reduction of the hydride catalyst amount. Overall, our results significantly deepen the mechanistic understanding of the FCR and potentially allow for a better and more sustainable process. Moreover, our work will help accelerate the development of new processes starting from CO_2-derived formates as carbon source.

Experimental Section

All reactions were performed in a purpose-built reactor, which can be operated using variable temperature gradients or pre-heated and reaches 700 °C. Glass vials with a volume of 15 mL were used as reactors at temperatures from 25–450 °C. The reactions were performed in argon atmosphere without purging but pressure relief via a vent port. The experimental series included reaction time, temperature, heating-rate, catalyst type, and catalyst loading as variables to understand mechanistic differences and find the catalysts delivering the highest yield at the lowest temperature in the shortest time possible. All chemicals were reagent grade and obtained from Sigma-Aldrich. Sample preparation included a drying of all reagents in a vacuum oven and introduction to an argon-filled glovebox at oxygen and water levels below 0.1 ppm. All catalyst and formate mixtures were prepared in 5 g batch sizes by

meticulous mixing using a mortar and pestle. Kinetic measurements were performed using an operando Raman spectrometer coupled with purpose-built bubble counting device for high-resolution gas quantification.[62] Quantitative analysis of solid products was performed by liquid-cell IR spectroscopy and LC measurements.

Acknowledgements

We thank the European commission for the funding from the European Union's Horizon 2020 research and innovation program under grant No. 767798.

Conflict of Interest

The authors declare no conflict of interest.

Keywords: CO_2 conversion · formate coupling · hydrides · polyester monomers · superbase catalysts

[1] Jullion, Crane, MacDougall, Rawson, *Polytech. J.* **1852**, *124*, 175–181.
[2] G. Laber, in *Ullmanns Enzyklopädie Der Technischen Chemie*, **1962**, pp. 51–55.
[3] P. A. Florio, in *Kirk-Othmer Encyclopedia of Chemical Technology, 2nd ed.*, Interscience Publishers, **1967**, pp. 356–373.
[4] J. Bollen, in *Designing Sustainable Technologies, Products and Policies*, Springer International Publishing, Cham, **2018**, pp. 307–309.
[5] M. Aresta, *Carbon Dioxide as Chemical Feedstock*, **2010**.
[6] *Putting CO_2 to Use - Creating Value from Emissions*, Paris, **2019**.
[7] P. Styring, E. A. Quadrelli, K. Armstrong, *Carbon Dioxide Utilisation*, Elsevier, **2015**.
[8] A. Raza, R. Gholami, R. Rezaee, V. Rasouli, M. Rabiei, *Petroleum* **2019**, *5*, 335–340.
[9] E. S. Gnanakumar, N. Chandran, I. V. Kozhevnikov, A. Grau-Atienza, E. V. Ramos Fernández, A. Sepulveda-Escribano, N. R. Shiju, *Chem. Eng. Sci.* **2019**, *194*, 2–9.
[10] M. Ronda-Lloret, G. Rothenberg, N. R. Shiju, *ChemSusChem* **2019**, *12*, 3896–3914.
[11] F. Jin, Y. Gao, Y. Jin, Y. Zhang, J. Cao, Z. Wei, R. L. Smith, *Energy Environ. Sci.* **2011**, *4*, 881–884.
[12] H. Zhong, L. Wang, Y. Yang, R. He, Z. Jing, F. Jin, *ACS Appl. Mater. Interfaces* **2019**, *11*, 42149–42155.
[13] M. Jouny, W. Luc, F. Jiao, *Ind. Eng. Chem. Res.* **2018**, *57*, 2165–2177.
[14] R. Aldaco, I. Butnar, M. Margallo, J. Laso, M. Rumayor, A. Dominguez-Ramos, A. Irabien, P. E. Dodds, *Sci. Total Environ.* **2019**, *663*, 738–753.
[15] F. D. Meylan, V. Moreau, S. Erkman, *J. CO_2 Util.* **2015**, *12*, 101–108.
[16] R. M. Cuéllar-Franca, A. Azapagic, *J. CO_2 Util.* **2015**, *9*, 82–102.
[17] J. Artz, T. E. Müller, K. Thenert, J. Kleinekorte, R. Meys, A. Sternberg, A. Bardow, W. Leitner, *Chem. Rev.* **2018**, *118*, 434–504.
[18] K. Roh, H. Lim, W. Chung, J. Oh, H. Yoo, A. S. Al-Hunaidy, H. Imran, J. H. Lee, *J. CO_2 Util.* **2018**, *26*, 60–69.
[19] I. A. G. Wilson, P. Styring, *Front. Energy Res.* **2017**, *5*, DOI: 10.3389/fenrg.2017.00019.
[20] M. A. Murcia Valderrama, R.-J. van Putten, G.-J. M. Gruter, *Eur. Polym. J.* **2019**, *119*, 445–468.
[21] "Oxalic acid from CO2 using Eletrochemistry At demonstratioN scale | OCEAN Project | H2020 | CORDIS | European Commission", can be found under https://cordis.europa.eu/project/id/767798, **2020**.
[22] A. R. T. Morrison, V. Van Beusekom, M. Ramdin, L. J. P. V. Broeke, T. J. H. Vlugt, W. Jong, *J. Electrochem. Soc.* **2019**, *166*, E77–E86.
[23] R. C. Weast, *CRC Handbook of Chemistry, and Physics*, Boca Raton, **1989**.
[24] W. Riemenschneider, M. Tanifuji, in *Ullmann's Encyclopedia of Industrial Chemistry*, Wiley-VCH, **2012**, pp. 529–541.
[25] R. Setton, *Bull. Soc. Chim. Fr.* **1958**, *11–12*.
[26] J. H. H. Meurs (Shell Internationale Research Maatschappij B. V.), WO 2016/124646 A1, **2016**.
[27] J. J. Kaczur, P. P. Lakkaraju, R. R. Parajuli (Avantium Knowledge Centre B. V.), WO2017121887 A1, **2017**.
[28] L. K. Freidlin, A. A. Balandin, A. I. Lebedeva, *Russ. Chem. Bull.* **1941**, *2*.
[29] L. K. Freidlin, *Z. Obs. Khimii* **1937**, *7*, 1675–1683.
[30] L. K. Freidlin, A. A. Balandin, A. I. Lebedeva, **1940**, *6*, 955–962.
[31] L. K. Freidlin, *Prom-st. Org. Khim.* **1937**, *3*, 681–686.
[32] L. K. Freidlin, *Z. Prikl. Khimii* **1938**, *11*, 975–980.
[33] A. A. Balandin, L. K. Freidlin, D. N. Vaskevich, *Sci. Rep.* **1936**, *6*, 321–345.
[34] L. K. Freidlin, A. A. Balandin, A. I. Lebedeva, *Russ. Chem. Bull.* **1941**, *2*, 261–267.
[35] L. K. Freidlin, *Z. Prikl. Khimii* **1937**, *10*, 1086–1094.
[36] L. K. Freidlin, A. A. Balandin, A. I. Lebedeva, *Russ. Chem. Bull.* **1941**, *2*, 255–262.
[37] A. A. Balandin, L. K. Freidlin, *Z. Obs. Khimii* **1935**, *6*, 868–872.
[38] L. K. Freidlin, A. A. Balandin, A. I. Lebedeva, *Russ. Chem. Bull.* **1941**, *2*, 268–274.
[39] L. K. Freidlin, *Trans. All-Union Acad. Food Ind. named after Stalin* **1939**, 145–157.
[40] L. K. Freidlin, **Scientific reports of Moscow university 1936**, 152–156.
[41] S. Shishido, Y. Masuda, *Nippon Kagaku Kaishi* **1976**, *1*, 66–70.
[42] S. Shishido, Y. Masuda, *Nippon Kagaku Kaishi* **1973**, *I*, 185–188.
[43] A. Górski, A. Kraśnicka, *J. Therm. Anal.* **1987**, *32*, 1243–1251.
[44] A. Górski, A. D. Kraśnicka, *J. Therm. Anal.* **1987**, *32*, 1229–1241.
[45] A. Górski, A. D. Kraśnicka, *J. Therm. Anal.* **1987**, *32*, 1895–1904.
[46] A. Górski, A. D. Kraśnicka, *J. Therm. Anal.* **1987**, *32*, 1345–1354.
[47] X. Yu, CN1502599 A, **2004**.
[48] K. Xie (University of Electronic Science and Technology of China), CN1727322A, **2006**.
[49] Q. Ma, A. Li, Y. Li (Taiyuan University of Technology), CN100999462A, **2007**.
[50] A. Li, Y. Li (Taiyuan University of Technology), CN1927805A, **2007**.
[51] A. Li, C. Liu, Q. Li (Taiyuan University of Technology), CN101077855A, **2007**.
[52] Z. Cao, Y. Cao, CN201343509Y, **2009**.
[53] Z. Cao, Y. Cao, CN101462943A, **2009**.
[54] A. Li, Y. Li (Taiyuan University of Technology), CN101823950A, **2010**.
[55] H. Jiang, D. Li, Z. Jiang, D. Wang, Z. Ban, B. Zhang (Tianjin Tanyi Synthesis Engineering Carbon Co., Ltd.), CN102659556A, **2012**.
[56] A. Li, Y. Li, Z. Zhao, A. Zhang, Z. Li (Taiyuan University of Technology), CN1903821B, **2012**.
[57] Z. Xu, X. Cheng, W. Xia (Luotian County Fuyang Chemical Fertilizer Co., Ltd.), CN102391099A, **2012**.
[58] Q. Guo (Ningxia Hainachuan Chemical Technology Co., Ltd.), CN107216248A, **2017**.
[59] P. S. Lakkaraju, M. Askerka, H. Beyer, C. T. Ryan, T. Dobbins, C. Bennett, J. J. Kaczur, V. S. Batista, *ChemCatChem* **2016**, *8*, 3453–3457.
[60] V. Merz, W. Weith, *Berichte der Dtsch. Chem. Gesellschaft* **1882**, *15*, 1507–1513.
[61] M. Goldschmidt, *Process of Making Oxalates*, **1900**, US659733.
[62] T. K. Slot, N. R. Shiju, G. Rothenberg, *Angew. Chem. Int. Ed.* **2019**, *58*, 17273–17276; *Angew. Chem.* **2019**, *131*, 17433–17436.
[63] A. Wiens (Elektrochemische Werke Bitterfeld), US714347, **1902**.
[64] L. W. Andrews, US1281117, **1918**.
[65] M. Enderli, A. Schrodt (Rudolph Koepp & Co. Chemische Fabrik AG), US2033097, **1936**.
[66] E. Hene (Rudolph Koepp & Co. Chemische Fabrik AG), US2004867, **1935**.
[67] A. Banerjee, M. W. Kanan, *ACS Cent. Sci.* **2018**, *4*, 606–613.
[68] B. Goldstein, H. Levine, D. Torney, *SIAM J. Appl. Math.* **2007**, *67*, 1147–1165.
[69] K. Hartman, I. C. Hisatsune, *J. Phys. Chem.* **1966**, *583*, 1281–1287.

Manuscript received: November 25, 2020
Revised manuscript received: January 5, 2021
Accepted manuscript online: January 11, 2021
Version of record online: February 2, 2021